Available online at www.sciencedirect.com
ScienceDirect
Trans. Nonferrous Met. Soc. China 33(2023) 2535−2542
Transactions of Nonferrous Metals Society of China
www.tnmsc.cn

Selective separation of La(III) and Ce(III) from aqueous solution by rotating disk membrane

Dan-dan LU[1], Jing GAO[1,2], Han ZHOU[1], Yun-ren QIU[1]

1. School of Chemistry and Chemical Engineering, Central South University, Changsha 410083, China;
2. Changsha Research Institute of Mining and Metallurgy Co., Ltd., Changsha 410012, China

Received 29 April 2022; accepted 21 October 2022

Abstract: To selectively separate La(III) and Ce(III) from aqueous solution, complexation−ultrafiltration and shear induced dissociation coupling with ultrafiltration were adopted with rotating disk membrane (RDM) and complexing agent polyacrylate sodium (PAAS). The effects of mass ratio of PAAS to rare earth ions (m(P)/m(RE)) and pH on rare earth rejection were investigated, and the suitable conditions of m(P)/m(RE)=4.0 and pH 5.0−7.0 were obtained. The critical shear rates of PAA-La and PAA-Ce complexes were 8.5×10^4 and 9.0×10^4 s^{-1} at pH 5.0, respectively. Frontier orbital theory was employed to obtain the energy gap value (ΔE) of the complexes. The results showed that PAA-Ce complex was more stable, which was consistent with the results of the critical shear rate. The maximum selective separation coefficient ($\beta_{La/Ce}$) arrived at 49.3 and 16.6 under the rotating rate of 1500 r/min at pH 5.0 and 6.0, respectively. Finally, the complexation property of regenerated PAAS was studied.

Key words: selective separation; rare earth; rotating disk membrane; complexation; ultrafiltration; shear induced dissociation

1 Introduction

Rare earth elements, with the good name of "industrial vitamins", are widely used in military, electronics, petrochemical, metallurgy and other fields due to their excellent optical, electrical, magnetic and other special properties. China's rare earth reserves occupy the first place in the world, and their development and utilization have become a research hotspot [1,2]. Solvent extraction is currently used for the separation of rare earth ions [3−5], but there also exist some disadvantages such as low efficiency of one-stage extraction, high consumption of acid and alkali in saponification treatment, and loss of organic solvent. Therefore, it is necessary to develop a novel separation method with green and high efficiency for the long-term sustainability of rare earth industry [6−10].

Complexation−ultrafiltration (C-UF) is a typical membrane separation technology for the separation of heavy metal ions from wastewater [11−13]. REN et al [14] used palygorskite to treat heavy metals in wastewater by complexation-ultrafiltration under different pH values and ionic strengths. The rejections of Cu, Zn and Cd could reach over 86.8%, 93.6% and 93.7%, respectively. REZANIA et al [15] synthesized PITA as a complexing agent and used it in an ultrafiltration process to remove Pb(II) in synthetic water. However, there still exists low efficiency in selective separation of metal ions in complexation−ultrafiltration process, and it consumes large amount of acid and alkali in the subsequent dissociation of the polymer-metal complex and the recovery of the metal ions [16,17].

The shear induced dissociation coupling with

Corresponding author: Yun-ren QIU, Tel: +86-13507479124, E-mail: csu_tian@csu.edu.cn
DOI: 10.1016/S1003-6326(23)66279-X

ultrafiltration (SID-UF) reveals outstanding advantages in the separation and recovery of heavy metal ions from wastewater [18,19]. It achieves high selective separation of metal ions according to the difference of shear stabilities among different polymer-metal complexes [20]. Rotating disk membrane (RDM) can produce adjustable shear field and create a powerful shear force on the membrane surface by the rotating disk. The strong shear action makes it difficult for the pollutant to deposit on the membrane surface, and can effectively reduce the concentration polarization and the adsorption fouling [21,22]. SID-UF is regarded as a promising separation technique because of its high separation efficiency and environmental friendliness.

In this work, La(III) and Ce(III) in aqueous solution were separated using polyacrylate sodium (PAAS) as complexing agent by RDM complexation−ultrafiltration technology. The effects of rotating speed, pH and mass ratio of PAAS to rare earth ions (m(P)/m(RE)) on La(III) and Ce(III) rejections were studied in C-UF. Furthermore, the shear stabilities of PAA-RE(La,Ce) complexes were investigated, and the critical shear rates were obtained. The selective separation of La(III) and Ce(III) and the regeneration of PAAS were realized by SID-UF.

2 Experimental

2.1 Materials and apparatus

Sodium polyacrylate (PAAS, with relative molecular mass of 2.5×10^5) was obtained from Tianjin Guangfu Fine Chemical Research Institute, China. The structural formula is shown in Fig. 1. A hollow fiber ultrafiltration membrane with the relative molecular mass of 2×10^5 was used to remove small molecules in PAAS. A polyether sulfone (PES) flat ultrafiltration membrane with a relative molecular mass cut-off (MWCO) of 1×10^4 was used for complexation and ultrafiltration (Tianjin Aisheng Membrane Filtration Technology Co., Ltd., China). La(III) and Ce(III) were derived from lanthanum oxide and cerium sulfate tetrahydrate, respectively. Appropriate additions of sodium hydroxide (0.1 mol/L) and hydrochloric acid (0.1 mol/L) were used to adjust the pH of the solution. All experimental agents were analytically grade and all solutions were prepared with deionized water.

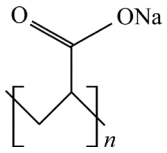

Fig. 1 Structure of PAAS

The experimental device module is shown in Fig. 2, wherein, a rotatable stainless steel disk with four blades was embedded in the vertical cavity shell. The feed port was set at the left 2/3 radius of the cavity shell, and the reflux liquid port and permeate port were located at the right center and 1/3 radius of the cavity shell, respectively. An electric motor was connected to one side of the housing to drive the disk to rotate. The polyethersulfone ultrafiltration membrane (outer diameter of 17.6 cm, inner diameter of 1 cm, and effective area of 0.0253 m^2) was attached to the stainless steel felt of the same size and fixed on the inner wall of the right cavity shell in front of the rotating disk. The rotating speed (N) of the rotating disk can be adjusted from 0 to 3000 r/min.

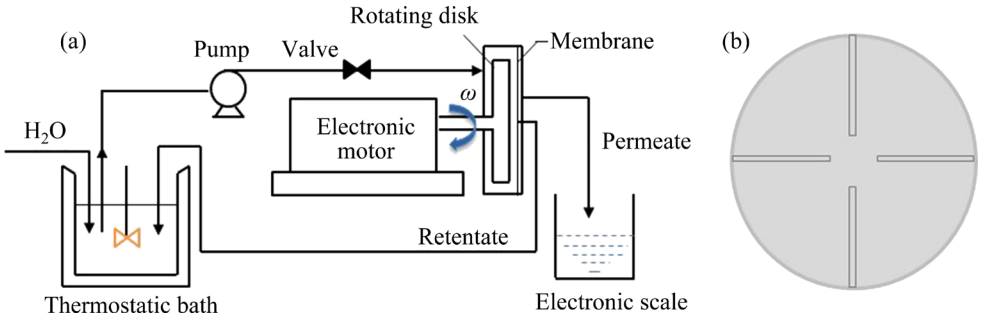

Fig. 2 Schematic diagram of shear enhanced ultrafiltration: (a) Operation diagram of shear enhanced ultrafiltration system; (b) Rotating disk with four blades

2.2 Ultrafiltration process

The feed was transferred from the feed tank with thermostatic bath into the rotating disk membrane module by a peristaltic pump, as shown in Fig. 2. In all experiments, the concentration of initial rare earth ions was 10 mg/L and feed flow rate was 12 L/h. The rotating speed was set as 50 r/min in C-UF. The rotating speed was adjusted and the permeate was collected for analysis after the system ran stably in SID-UF. Equivalent ultrapure water was added to the feed tank to maintain constant volume when the permeate was continuously removed throughout the experiment. All tests were repeated at least three times.

2.3 Calculation of critical shear rate and critical radius

The shear rate on the membrane surface increases with increasing rotating speed at the same radius, and it increases with increasing radius at a certain rotating speed. BOUZERAR et al [23] solved the axisymmetric equation and obtained the shear rate formula on the rotating disk. The formulas are as follows:

$$\gamma_{ml} = 0.77v^{-0.5}(k\omega)^{1.5}r \quad (1)$$

$$\gamma_{mt} = 0.0296v^{-0.8}(k\omega)^{1.8}r^{1.6} \quad (2)$$

where γ_{ml} and γ_{mt} represent the shear rates of the rotating disk in laminar and turbulent flow regimes, respectively; v represents the kinematic viscosity of the solution; ω is the angular velocity of the rotating disk; r stands for radius; k is the speed factor, which depends only on the geometry of the device.

The critical shear rate (γ_c) is the smallest one at which the polymer-metal complex begins to dissociate. Different complexes have different critical shear rates. According to Ref. [24], a segmentation model has been established, as shown in Fig. 3(a), where r_i and r_o are the inner and outer radii of the membrane, respectively. The membrane surface is divided into a complexation zone and a dissociation zone, as shown in Fig. 3(b). The critical shear rate and critical radius could be calculated according to the mass balance [21].

3 Results and discussion

3.1 Effect of *m*(P)/*m*(RE)

The effects of *m*(P)/*m*(RE) on the rejections (*R*) of La(III) and Ce(III) in C-UF are shown in Fig. 4. It is obvious that the rejections of La(III) and Ce(III) increase with the addition of PAAS at the initial stage. In Fig. 4(a), the rejection exceeds 99% at *m*(P)/*m*(RE)=4.0 and gradually stabilizes at pH 5.0. The rejections of rare earth ions increase constantly as more RE ions can combine with PAAS with the addition of PAAS. Almost all the rare earth ions completely combine with PAAS when excessive PAAS is added, and the rejection is near 100%.

It can be seen from Fig. 4(b) that both the rejections of La(III) and Ce(III) increase with the increase of *m*(P)/*m*(RE), but the rejection of La(III) is a little smaller than that of Ce(III). The rejection of Ce(III) is approximately 44% and La(III) is about 40% at *m*(P)/*m*(RE)=0.8. Ce(III) is almost completely complexed at *m*(P)/*m*(RE)=2.0, while La(III) is done at *m*(P)/*m*(RE)=2.4.

3.2 Effect of pH

pH has an important influence on the complexation in solution and the charge on the membrane surface. Figure 5 shows the effect of pH on the rejection at *m*(P)/*m*(RE)=4.0. As the pH rises, the rejections of La(III) and Ce(III) are gradually increased up to 99%. Due to very similar chemical properties of rare earth elements, indicating that pH plays a significant role in the separation of La(III)

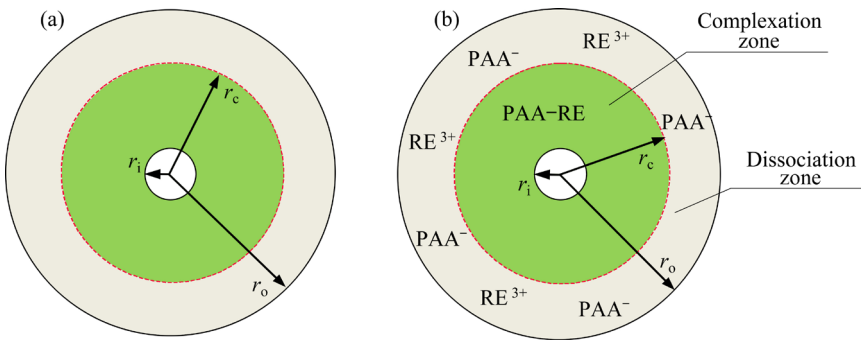

Fig. 3 Membrane surface segmentation diagram (a) and distribution form of RE on membrane surface (b)

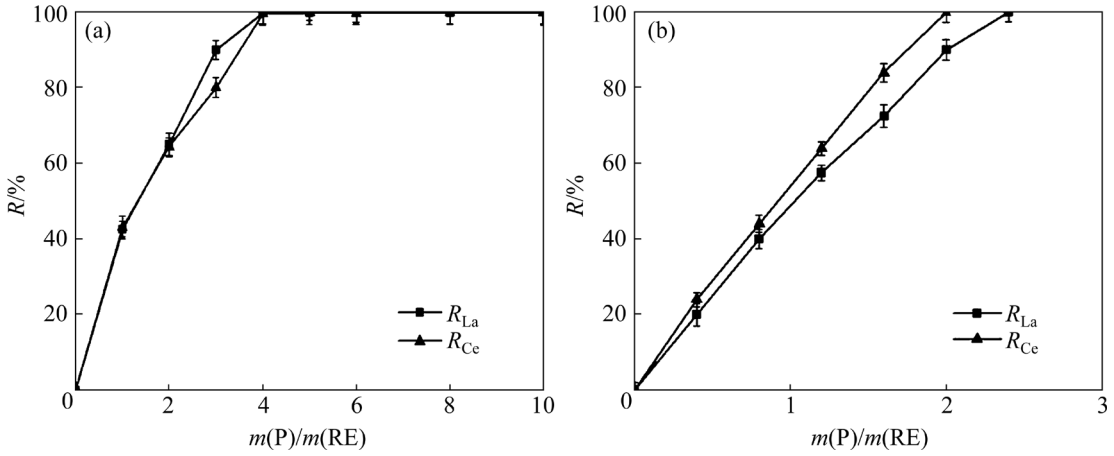

Fig. 4 Influence of m(P)/m(RE) on rejections of single RE ions (a) and mixed RE ions (b)

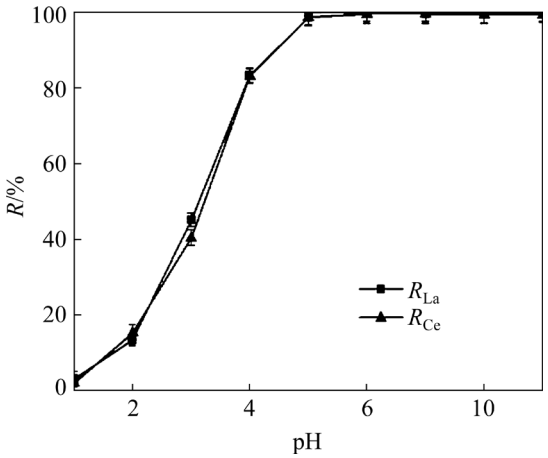

Fig. 5 Influence of pH on PAA-RE rejection

and Ce(III). Massive hydrogen ions will combine with PAA^- and reduce the complexation sites with RE ions at low pH. With the increase of pH, more rare earth ions will combine with PAA^- and form PAA-RE complexes, and the rejection increases. However, rare earth ions may form hydroxide precipitate when pH is greater than 5.0 and deposit on the membrane surface. Thus, pH 5.0 is chosen as the suitable condition.

3.3 Effect of shear rate

3.3.1 Dissociation of PAA-RE complexes at different m(P)/m(RE)

The PAA-RE complexes begin to dissociate when the rotating disk reaches a certain rotating speed, i.e. the critical rotating speed (N_c). After dissociation, the free rare earth ions pass through the membrane, resulting in the decrease of rejection. Figure 6 shows the influence of m(P)/m(RE) and rotating speed (N) on the shear stability of PAA-La and PAA-Ce complexes at pH 5.0.

In Fig. 6(a), when N is below 1520 r/min, the rejection of La(III) remains constant, but the rejection decreases rapidly when the speed is greater than 1520 r/min. Therefore, the N_c of PAA-La complex is 1520 r/min. Similarly, as seen from Fig. 6(b), the N_c of PAA-Ce complex is 1570 r/min. The critical shear rates of PAA-La and PAA-Ce complexes were calculated as 8.5×10^4 and $9.1\times10^4\ s^{-1}$ at pH 5.0, respectively. The N_c of PAA-RE complexes remains unchanged regardless of m(P)/m(RE), showing that m(P)/m(RE) has no effect on the stabilities of the complexes.

3.3.2 Dissociation of PAA-RE complexes at different pH

It can be seen from Fig. 7 that the rejections of La(III) and Ce(III) have the same change trend at pH 7.0, 6.0, and 5.0. The critical rotating speeds of PAA-La and PAA-Ce complexes are 1520 and 1570 r/min at pH 5.0, respectively, 1470 and 1530 r/min at pH 6.0, respectively, and 1300 and 1480 r/min at pH 7.0, respectively. At the same pH, the N_c of PAA-La complex is lower than that of PAA-Ce complex.

The complexation of PAAS and rare earth ions and dissociation of PAA-RE complexes are reversible. pH affects the complexation of RE ions with PAAS as well as the dissociation of PAA-RE complexes. The increase of H^+ improves the competitive combination with complexing agent and enhances the dissociation of PAA-RE complexes. However, high shear action generated by the rotating disk at high speeds may cause the dissociation of PAA-RE complexes. The greater the rotating speed is, the larger the dissociation area on the membrane surface is [24].

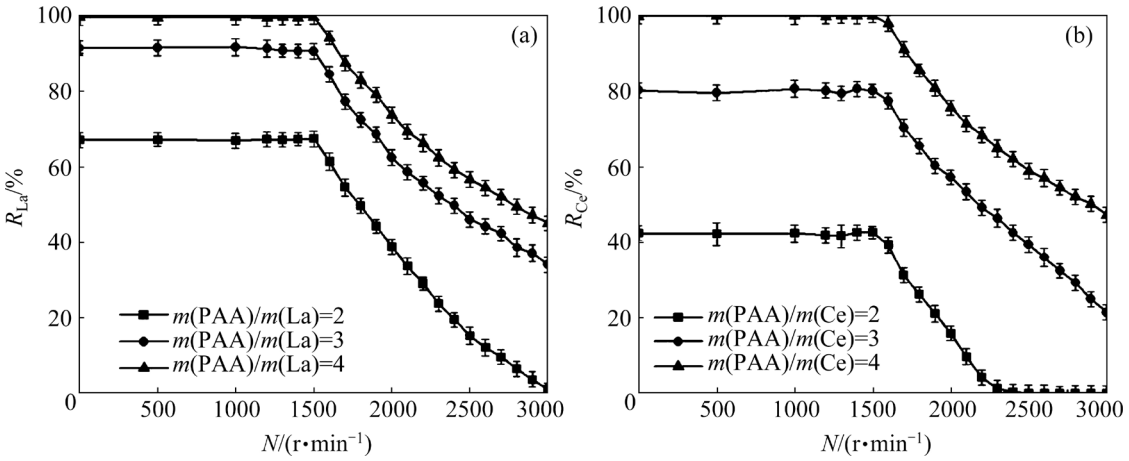

Fig. 6 Influence of m(P)/m(RE) on PAA-RE shear stability: (a) PAA-La; (b) PAA-Ce

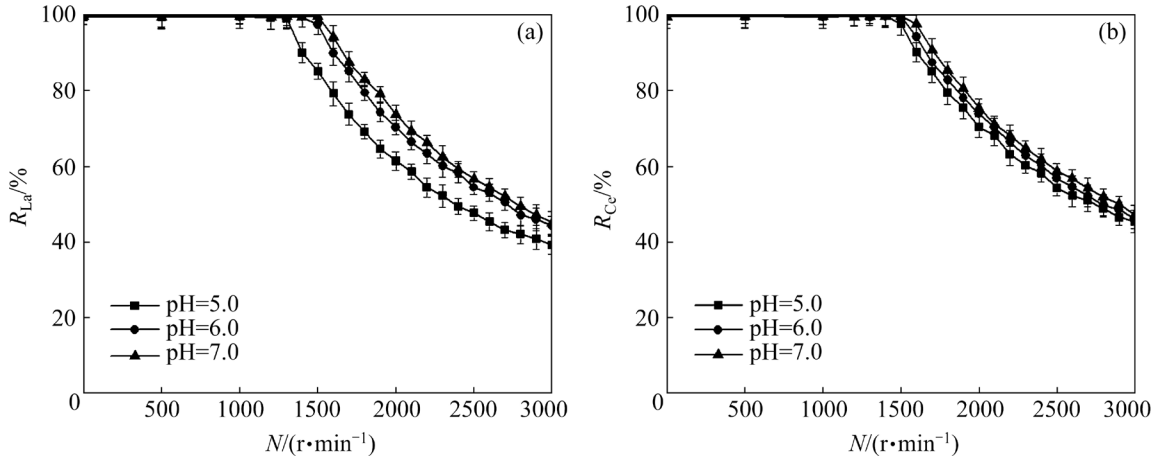

Fig. 7 Influence of pH on PAA-RE shear stability: (a) PAA-La; (b) PAA-Ce

Previous studies have proved that the complexing agent can still maintain a complete molecular chain even at high rotating speeds. Therefore, the decrease of rejection is attributed to the breaking of coordination bond of PAA-RE complexes [20]. It can be seen from the above that the PAA-Ce complex is more stable than PAA-La complex in the shear field.

3.3.3 Separation coefficient of La(III) and Ce(III)

The separation coefficient of two RE ions (La(III) and Ce(III)) is expressed as $\beta_{La/Ce}$ as follows [25]:

$$\beta_{La/Ce}=\left(\frac{C_{p,La}}{C_{f,La}}\right)\left(\frac{C_{f,Ce}}{C_{p,Ce}}\right)=\frac{1-R_{La}}{1-R_{Ce}} \quad (3)$$

where $C_{p,La}$ and $C_{p,Ce}$ represent the concentrations of La(III) and Ce(III) ions in the permeate (mg/L), respectively; $C_{f,La}$ and $C_{f,Ce}$ indicate the initial concentrations of La(III) and Ce(III) ions in the feed (mg/L), respectively.

It can be seen from Fig. 8 that the separation coefficient of La(III) and Ce(III) increases with increasing the rotating speed. It gradually reaches the maximum and then decreases to a smallest value near 1.0. PAA-La complex begins to dissociate when the shear rate reaches its γ_c, leading to a decrease of rejection. However, Ce(III) still exists in the solution

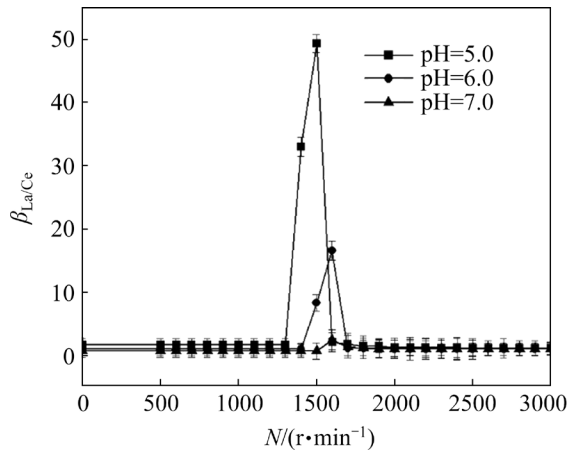

Fig. 8 Separation coefficients of La(III) and Ce(III) at different rotating speeds

as PAA-Ce complex, so $\beta_{La/Ce}$ gradually increases. When the shear rate reaches the γ_c of PAA-Ce complex, the rejection of Ce(III) begins to decrease, resulting in the reduction of $\beta_{La/Ce}$. Therefore, selective separation can be achieved by adjusting an appropriate shear rate.

When the solution pH is 5.0 and 6.0, the maximum separation coefficients of La(III) and Ce(III) and the corresponding rotating speeds are 49.3, 16.6 and 1500, 1600 r/min, respectively. As can be seen from Fig. 8, the separation coefficient reaches its maximum at pH 5.0.

3.3.4 Regeneration of PAAS

PAA-La complexes begin to dissociate at 1520 r/min and pH 5.0, and the free La(III) ions can permeate the membrane. After almost all the PAA-La complexes have dissociated and little La(III) ions are found in the permeate, the rotating speed is adjusted up to 1570 r/min, PAA-Ce complexes begins to dissociate, and the La(III) and Ce(III) are separated. After almost all the PAA-Ce complexes have dissociated and little Ce(III) ions are found in the permeate, the PAAS is regenerated in the retentate. The regenerated PAAS can be reused. The results of the 15 times of regeneration of PAAS are shown in Fig. 9. It is clearly seen that the rejections of La(III) are about 98% by using regenerated PAAS, which indicates that the regenerated PAAS has almost the same complexation property as the original PAAS.

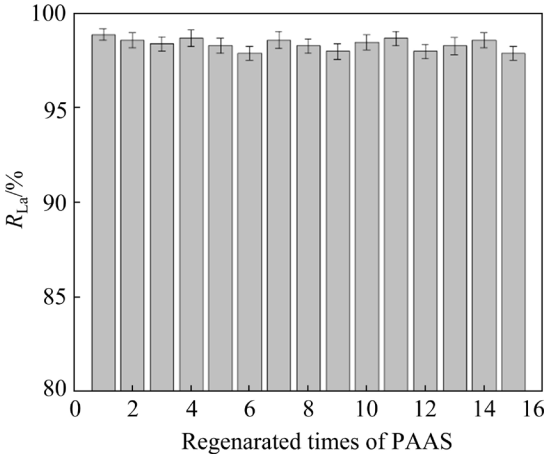

Fig. 9 Effect of regenerated PAAS on La(III) rejection

3.4 Stability of PAA-RE complex

In order to further verify the shear stability of PAA-RE complexes, the combination of RE with PAAS has been calculated using the DMol3 electronic structure code (Materials Studio 2019) based on the density functional theory GGA/BLYP/DNP. All atoms were selected to the all-electron double numerical polarization group (DNP). The complex was optimized with convergence accuracy of 1.0×10^{-5}.

The energy gap (ΔE) of PAA-RE complex has been calculated based on the energy of type and frontier orbital theory (HOMO and LUMO).

$$\Delta E=E_{HOMO}-E_{LUMO} \quad (4)$$

where E_{HOMO} and E_{LUMO} are the highest occupied molecular orbital energy and the lowest unoccupied orbital energy, respectively.

The stable configuration and frontier orbital theory distribution diagram of PAA-RE complexes are shown in Fig. 10. The frontier orbital theory energy of PAAS and rare earth ions complex is shown in Table 1.

The energy gap ΔE reflects the ability of electrons to transfer from an occupied orbit to an empty orbit in a chemical reaction. Generally, the higher the energy gap, the stronger the interaction force between the complexing agent and RE ions,

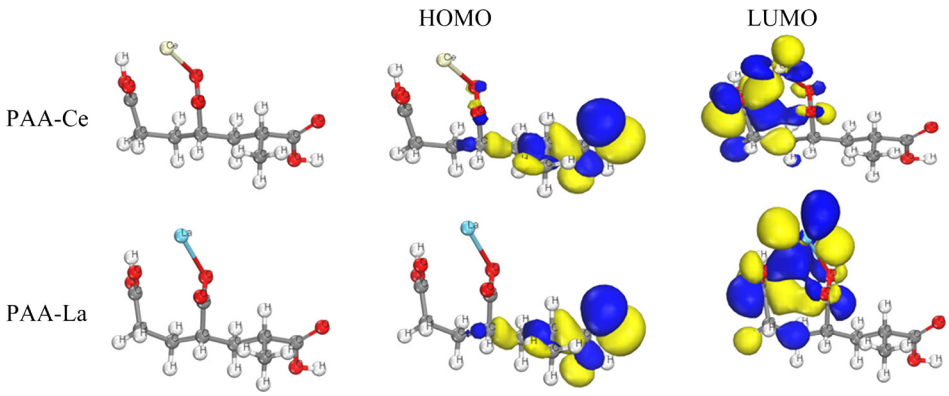

Fig. 10 Stable configuration, HOMOs and LUMOs of PAA-RE

Table 1 Frontier orbital energy of PAA-RE complexes

Complex	E_{HOMO}/eV	E_{LUMO}/eV	ΔE/eV
PAA-Ce	−8.5130	−6.1917	2.3213
PAA-La	−8.0060	−5.7481	2.2579

and the more stable the structure [26,27]. From Table 1, the energy gaps of PAA-Ce complex and PAA-La complex are 2.3213 and 2.2579 eV, respectively. It can be seen that the stability order of PAA-RE complexes from high to low is PAA-Ce > PAA-La. This is consistent with the experimental results.

4 Conclusions

(1) The effects of pH and m(P)/m(RE) on the rejections of RE ions were investigated by complexation−ultrafiltration, and the suitable conditions were m(P)/m(RE)=4.0 and pH 5.0−7.0.

(2) Stabilities of PAA-RE complexes were studied in the shear field at pH 5.0, and the critical shear rates of PAA-La and PAA-Ce complexes were 8.5×10^4 and 9.0×10^4 s^{-1}, respectively. This indicated that the PAA-Ce complex was more stable than PAA-La complex in the shear field, which was confirmed by frontier orbital theory.

(3) The effects of operating parameters on the selectivity separation coefficient ($\beta_{La/Ce}$) were studied. The maximum $\beta_{La/Ce}$ arrived at 49.3 and 16.6 under the rotating rate 1500 r/min at pH 5.0 and 6.0, respectively. La(III) and Ce(III) could be separated efficiently when the rotating speed was adjusted between the critical shear rates of PAA-La and PAA-Ce complexes.

(4) The regeneration of PAAS was achieved by SID-UF and the regenerated PAAS showed almost the same complexation property as the original one.

Acknowledgments

This work was supported by the National Natural Science Foundation of China (No. 22178392), and the Fundamental Research Funds for the Central Universities of Central South University, China (No. 2022ZZTS0493).

References

[1] ILYAS S, KIM H, SRIVASTAVA R R, CHOI S. Cleaner production of rare earth elements from phosphorus-bearing sulfuric acid solution of vein deposit monazite [J]. Journal of Cleaner Production, 2021, 278: 123435.

[2] LI D Q. Development course of separating rare earths with acid phosphorus extractants: A critical review [J]. Journal of Rare Earths, 2019, 37: 468−486.

[3] KASHI E, HABIBPOUR R, GORZIN H, MALEKI A. Solvent extraction and separation of light rare earth elements (La, Pr and Nd) in the presence of lactic acid as a complexing agent by Cyanex 272 in kerosene and the effect of citric acid, acetic acid and Titriplex III as auxiliary agents [J]. Journal of Rare Earths, 2018, 36: 317−323.

[4] FU Xuan, ZHANG Fang, WU Qiang, LI Yang, HUANG Qing-gang, YAN Ze-yi. The separation of thorium and rare earth elements using [A336][NO_3]: Insight into a new extraction mechanism [J]. Journal of Radioanalytical and Nuclear Chemistry, 2021, 327: 1251−1258.

[5] ILYAS S, KIM H, SRIVASTAVA R R. Extraction equilibria of cerium(IV) with Cyanex 923 followed by precipitation kinetics of cerium(III) oxalate from sulfate solution [J]. Separation and Purification Technology, 2021, 254: 117634.

[6] BALARAM V. Rare earth elements: A review of applications, occurrence, exploration, analysis, recycling, and environmental impact [J]. Geoscience Frontiers, 2019, 10: 1285−1303.

[7] WANG Jun-lian, LIU Lu, XU Guo-dong, WANG Pei-long, HUANG Guo-yong, YU Feng-shan. New compound N-methyl-N-isopropyl octanthioamide for palladium selective extraction and separation from chloride media [J]. Transactions of Nonferrous Metals Society of China, 2023, 33: 1609−1618.

[8] TENG Qing, YANG Zhi-chao, WANG Hong-jun. Recovery of vanadium and nickel from spent-residue oil hydrotreating catalyst by direct acid leaching-solvent extraction [J]. Transactions of Nonferrous Metals Society of China, 2023, 33: 325−336.

[9] HUANG Ting, WANG Yong-xi, HU Hui-ping, HU Fang, LUO Yu-qing, LIU Shi-jun. Phase separation in solvent extraction of cobalt from acidic sulfate solution using synergistic mixture containing dinonylnaphthalene sulfonic acid and 2-ethylhexyl 4-pyridinecarboxylate ester [J]. Transactions of Nonferrous Metals Society of China, 2019, 29: 1107−1116.

[10] CHEN Zi-ying, LI Zhan, CHEN Jia, KALLEM P, BANAT F, QIU Hong-deng. Recent advances in selective separation technologies of rare earth elements: A review [J]. Journal of Environmental Chemical Engineering, 2022, 10: 107104.

[11] HUMELNICU D, LAZAR M M, IGNAT M, DINU L A, DRAGAN E S, DINU M V. Removal of heavy metal ions from multi-component aqueous solutions by eco-friendly and low-cost composite sorbents with anisotropic pores [J]. Journal of Hazardous Materials, 2020, 381: 120980.

[12] WULAN P, KUSUMASTUTI Y, PRASETYA A. Removal of Fe(II) from aqueous solution by chitosan activated carbon composite beads [J]. Applied Mechanics and Materials, 2020, 898: 3−8.

[13] ZHOU Han, QIU Yun-ren, CHEN Yu-xin. Recovery of Hg(II) from aqueous solution by complexation-ultrafiltration using rotating disk membrane and shear stability of PMA-Hg complex [J]. Journal of Central South University, 2020, 27: 2507−2514.

[14] REN Jun, CAO Tian-yi, YANG Xin, TAO Ling. Ultrafiltration treatment of wastewater contained heavy metals complexed with palygorskite [J]. Polish Journal of Chemical Technology, 2020, 22: 1−9.
[15] REZANIA H, VATANPOUR V, FAGHANI S. Poly (itaconic acid)-assisted ultrafiltration of heavy metal ions' removal from wastewater [J]. Iranian Polymer Journal, 2019, 28: 1069−1077.
[16] PENG Xue-feng, ZHANG Yang, FAN Bing-qiang, ZHENG Shi-li, WANG Xiao-jian, ZHANG Ying, LI Ping, LIU Feng-qiang. Complexation separation for vanadium and chromium by dithiocarbamate and its application in treatment of chromium–vanadium-bearing slag [J]. Transactions of Nonferrous Metals Society of China, 2019, 29: 2400−2410.
[17] WU Hong-yang, HUANG Yan-fang, LIU Bing-bing, HAN Gui-hong, SU Sheng-peng, WANG Wen-juan, YANG Shu-zhen, XUE Yu-bin, LI Shuang-qing. An efficient separation for metal-ions from wastewater by ion precipitate flotation: Probing formation and growth evolution of metal-reagent flocs [J]. Chemosphere, 2021, 263: 128363.
[18] GAO Jing, QIU Yun-ren, HOU Ben, ZHANG Qiang, ZHANG Xiao-dong. Treatment of wastewater containing nickel by complexation-ultrafiltration using sodium polyacrylate and the stability of PAA-Ni complex in the shear field [J]. Chemical Engineering Journal, 2018, 334: 1878−1885.
[19] GAO Jing, QIU Yun-ren, LI Mao-lin, LE Hui-shang. Removal of Co(II) from aqueous solution by complexation−ultrafiltration and shear stability of PAA-Co complex [J]. Transactions of Nonferrous Metals Society of China, 2019, 29: 1346−1352.
[20] TANG Shu-yun, QIU Yun-ren. Removal of copper(II) ions from aqueous solutions by complexation–ultrafiltration using rotating disk membrane and the shear stability of PAA–Cu complex [J]. Chemical Engineering Research and Design, 2018, 136: 712−720.
[21] ZHANG Qiang, GAO Jing, QIU Yun-ren. Removal of Ni(II) and Cr(III) by complexation−ultrafiltration using rotating disk membrane and the selective separation by shear induced dissociation [J]. Chemical Engineering and Processing, 2019, 135: 236−244.
[22] COJOCARU C, CLIMA L H. Polymer assisted ultrafiltration of AO7 anionic dye from aqueous solutions: Experimental design, multivariate optimization, and molecular docking insights [J]. Journal of Membrane Science, 2020, 604: 118054.
[23] BOUZERAR R, DING L H, JAFFRIN M Y. Local permeate flux–shear–pressure relationships in a rotating disk microfiltration module: Implications for global performance [J]. Journal of Membrane Science, 2000, 170: 127−141.
[24] TANG Shu-yun, QIU Yun-ren. Selective separation and recovery of heavy metals from electroplating effluent using shear-induced dissociation coupling with ultrafiltration [J]. Chemosphere, 2019, 236: 124330.
[25] CHEN Zhi-peng, JIANG Zhao-hui, YANG Chun-jie, GUI Wei-hua, SUN You-xian. Dust distribution study at the blast furnace top based on k−Sε−up model [J]. Journal of Automatica Sinica, 2020, 8: 121−135.
[26] NJOKU D I, UKAGA I, IKENNA O B, OGUZIE E E, OGUZIE K L, IBISI N. Natural products for materials protection: Corrosion protection of aluminium in hydrochloric acid by Kola nitida extract [J]. Journal of Molecular Liquids, 2016, 219: 417−424.
[27] WAHAB O O, OLASUNKANMI L O, GOVEENDER K K, GOVEDER P P. DMol3/COSMO-RS prediction of aqueous solubility and reactivity of selected Azo dyes: Effect of global orbital cut-off and COSMO segment variation [J]. Journal of Molecular Liquids, 2018, 249: 346−360.

采用旋转圆盘膜技术从水溶液中选择性分离 La(III)和 Ce(III)

卢丹丹[1]，高 静[1,2]，周 韩[1]，邱运仁[1]

1. 中南大学 化学化工学院，长沙 410083；
2. 长沙矿冶研究院有限公司，长沙 410012

摘 要：以聚丙烯酸酯钠(PAAS)为络合剂，采用旋转圆盘膜(RDM)络合−超滤和剪切诱导解离耦合超滤的方法，从水溶液中选择性分离 La(III)和 Ce(III)。考察 PAAS 与稀土离子的质量比(m(P)/m(RE))和 pH 对离子截留率的影响，确定合适的络合条件为 m(P)/m(RE)=4.0 和 pH 5.0~7.0。 在 pH 5.0 的条件下，PAA-La 和 PAA-Ce 络合物的临界剪切速率分别为 8.5×10^4 和 9.0×10^4 s^{-1}。通过前线轨道理论对配合物的能量进行计算，得到能隙值 ΔE。结果表明，PAA-Ce 配合物更稳定，这与临界剪切速率的结果一致。在 pH 为 5.0 和 6.0、转速为 1500 r/min 时，两种离子的最大选择分离系数($\beta_{La/Ce}$)分别为 49.3 和 16.6。最后，考察再生 PAAS 的络合性能。

关键词：选择性分离；稀土；旋转盘膜；络合；超滤；剪切诱导解离

(Edited by Wei-ping CHEN)